



Density functional theory based computational investigations on the stability of highly active trimetallic PtPdCu nanoalloys for electrochemical oxygen reduction

Journal:	<i>Faraday Discussions</i>
Manuscript ID	FD-ART-05-2022-000101.R1
Article Type:	Paper
Date Submitted by the Author:	13-Jul-2022
Complete List of Authors:	Wang, Lichang; Southern Illinois University, Chemistry and Biochemistry Ore, Rotimi; Southern Illinois University Carbondale, Chemistry and Biochemistry Jayamaha, Peshala; Southern Illinois University Carbondale, Chemistry and Biochemistry Wu, Zhipeng; State University of New York at Binghamton, Chemistry Zhong, Chuan-jian; State University of New York at, Department of Chemistry

Density functional theory based computational investigations on the stability of highly active trimetallic PtPdCu nanoalloys for electrochemical oxygen reduction

Lichang Wang,^{1,*} Rotimi M. Ore,¹ Peshala K. Jayamaha,¹ Zhi-Peng Wu²
and Chuan-Jian Zhong²

¹*School of Chemical and Biomolecular Sciences and the Materials Technology Center, Southern Illinois University, Carbondale, IL 62901, USA*

²*Department of Chemistry, State University of New York at Binghamton, Binghamton, NY 13902, USA*

ABSTRACT

Activity, cost, and durability are the trinity of catalysis research for electrochemical oxygen reduction reaction (ORR). While studies towards increasing activity and reducing cost of ORR catalysts have been carried out extensively, much effort is needed in durability investigation of highly active ORR catalysts. In this work, we examined the stability of a trimetallic PtPdCu catalyst that has demonstrated high activity and incredible durability during ORR using density functional theory (DFT) based computations. Specifically, we studied the processes of dissolution/deposition and diffusion between surface and inner layer of Cu species of Pt₂₀Pd₂₀Cu₆₀ catalysts at electrode potentials up to 1.2 V to understand their role towards stabilizing Pt₂₀Pd₂₀Cu₆₀ catalysts. The results show there is a dynamic Cu surface composition range that is dictated by the interplay of the four processes, dissolution, deposition, diffusion from surface to inner layer, and diffusion from inner to surface layer of Cu species in the stability and observed oscillation of lattice constants of Cu-rich PtPdCu nanoalloys.

*Correspondence author: lwang@chem.siu.edu.

Introduction

Research on heterogeneous catalysis has centered on the investigations of three facets of catalysis: activity, cost, and durability. Although these three aspects of catalysis are closely correlated, the first phase of catalysis research often focuses on searching for highly active catalysts. Catalysis of ethanol oxidation is mainly at this stage of research due primarily to the complexity of the reaction:¹⁻³ There are 46 reaction pathways to remove H atom⁴⁻⁶ and 24 to break C-C bond⁶⁻⁸ in ethanol oxidation. Therefore, the complex reaction network of ethanol oxidation requires tremendous efforts to investigate the activities of a catalyst. On the other hand, catalysis studies of oxygen reduction reaction (ORR) have entered well into the second phase of research, i.e. reducing cost by reducing Pt usage⁹ or searching for Pt free¹⁰ or even metal free ORR catalysts.^{11, 12} Furthermore, efforts in the third phase of ORR catalysis, i.e. developing highly durable catalysts with high activity and low cost, have recently increased. Development of the highly active, cost-effective, and yet very durable Pt₂₀ Pd₂₀Cu₆₀ ORR catalysts is the result of such an effort.⁹

Durability of a catalyst can be affected by many factors, such as carbon corrosion, catalysts dissolution, and particle sintering.^{13, 14} For instance, sintering of Pt nanoparticles was found to be due to Ostwald ripening via the formation of volatile PtO₂¹⁵ or influence of crystal facets.¹⁶ Sintering can also occur when there are weak interactions between catalysts and their support.^{17, 18} In addition to sintering, dissolution is also another important factor related to the stability of catalysts.¹⁹ Experimentally, studies of nanoparticle during catalysis under operando conditions have provided invaluable information on the stability and transformation of catalysts.²⁰ Time-resolved dissolution study¹⁹ and imaging elemental inhomogeneity of nanoparticles²¹ are the most recent tools to investigate the stability of catalysts. Computationally, progress has been made in the study of degradation mechanism including using nonmonotonic dynamics theory to describe

the Ostwald ripening in nanoparticle catalysts²² and using DFT based methods to study dissolution²³ and model the correlation between stability of nanoparticles and the size, shape, and composition.²⁴

Alloying has been demonstrated as an effective strategy to enhance the stability of catalysts. For instance, PtNi-based catalysts²⁵ possess significantly enhanced stability for ORR and PdAu/Pt for methanol oxidation.²⁶ Furthermore, core-shell structure is often utilized to prevent leaching of non-noble metal from catalysts and therefore enhancing the durability of the catalyst. Examples of the core-shell catalysts are Cu@Pt,²⁷ Pt-Co@Pt,²⁸ Ni/PtAu,²⁹ and Cu@PtPd³⁰ that have exhibited great durability for ORR. The mechanism of utilizing core-shell structure is the formation of a protective Pt layer to enhance the catalyst durability. While the core-shell structure of nanoparticles provides good stability, Pt or PtPd content is often needed to be above 50% in order to form a shell for particles of 5 nm, which limits the efforts to further lowering the Pt usage. Alternative is to develop base-metal rich but random alloy nanoparticles beyond core-shell structure with a Pt or PtPd content of lower than 50%. This strategy is based on a different mechanism than that for the core-shell structure, that is the existence of a stable phase in the random alloy nanoparticles rather than core-shell structure at certain range of compositions. Explorations on the range of compositions with less than 50% of Pt or PtPd content of highly active catalysts would be crucial. Previous work indicated that such a strategy is feasible. For instance, doping Au clusters can enhance the stability of Pt nanoparticles.³¹ Introduction of a third metal Mo to Pt₃Ni nanoparticles³² also enhances their stability. Our expedition toward this led to the discovery of trimetallic Pt₂₀Pd₂₀Cu₆₀ nanoparticles show high active and durability for ORR.⁹

After 50,000 cycles of accelerated durability test, mass activity of Pt₂₀Pd₂₀Cu₆₀ nanoparticles still remained at 99.8% of the initial activity.⁹ Moreover, random alloy phase of the Pt₂₀Pd₂₀Cu₆₀

nanoparticles withstands during catalysis as shown from the high resolution high-angle annular dark-field scanning transmission electron microscopy and electron energy loss spectroscopy elemental mapping of the catalysts. With the encouraging results, it would be important to fully understand the mechanism of the high durability of these nanoparticles for future development of even better catalysts. As such, in this work, we performed density functional theory (DFT) based computations to study the highly active trimetallic Pt₂₀Pd₂₀Cu₆₀ nanoalloys in order to provide a molecular understanding of their high stability under electrochemical environments. The leading impetus of this work is to investigate the role of dissolution/deposition and interlayer diffusion of Cu species in the durability of Pt₂₀Pd₂₀Cu₆₀ nanoparticles.⁹

Specifically, we performed DFT calculations to obtain energetics related to the dissolution, deposition, and diffusion processes as shown in Fig. 1 at different electrode potentials. To explore the effect of surface composition to the stability of the nanoparticles, we fixed the overall composition of the nanoparticles at 20, 20, and 60 for Pt, Pd, and Cu, respectively but varied the surface compositions. Surface energy and free energies of the catalysts with different surface compositions were obtained. Using the DFT obtained energetics, we performed kinetics simulations to obtain the rates of these processes. We note that sintering process is not considered in this work based on the experimental observations, i.e. the size of nanoparticles changed only slightly from the initial ~5.5 nm to ~5.8 nm after 20,000 cycles.⁹

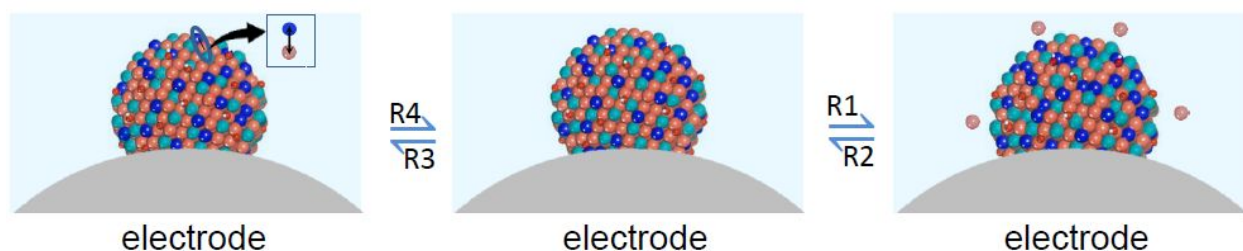


Fig. 1 Schematic description of dissolution (R1), deposition (R2), Cu interlayer diffusions, i.e. diffusion from surface to inner layers (R3) and diffusion from inner layers to surface (R4) in the PtPdCu nanoparticle under electrochemical environment. Brown, dark blue, and blue balls denote Cu, Pt, and Pd atoms, respectively. Red smaller balls represent adsorbed species such as H^{*}, OH^{*}, or O^{*} under different electrode potentials.

Methodology and computational details

The energetics of the dissolution/deposition and interlayer diffusions of Cu species of Pt₂₀Pd₂₀Cu₆₀ nanoparticles was obtained from DFT calculations. Experimentally, the nanoparticles are about 5.6 nm, which consists of ~5000 atoms. Furthermore, many low index facets, such as (111), (100), and (110), are present depending on the electrode potential. In this work, our model catalyst consists of a periodic slab with the (111) surface of PtPdCu with a composition of 18.75%(Pt), 18.75%(Pd), and 62.5%(Cu) and one of its configurations is shown in Fig. 2. The periodic slab has five layers with 15 Å of vertical vacuum space to eliminate the interaction between the slab and its periodic images. In the DFT calculations, the top two layers of the model catalysts were allowed to be fully relaxed without any constraints in the calculations.

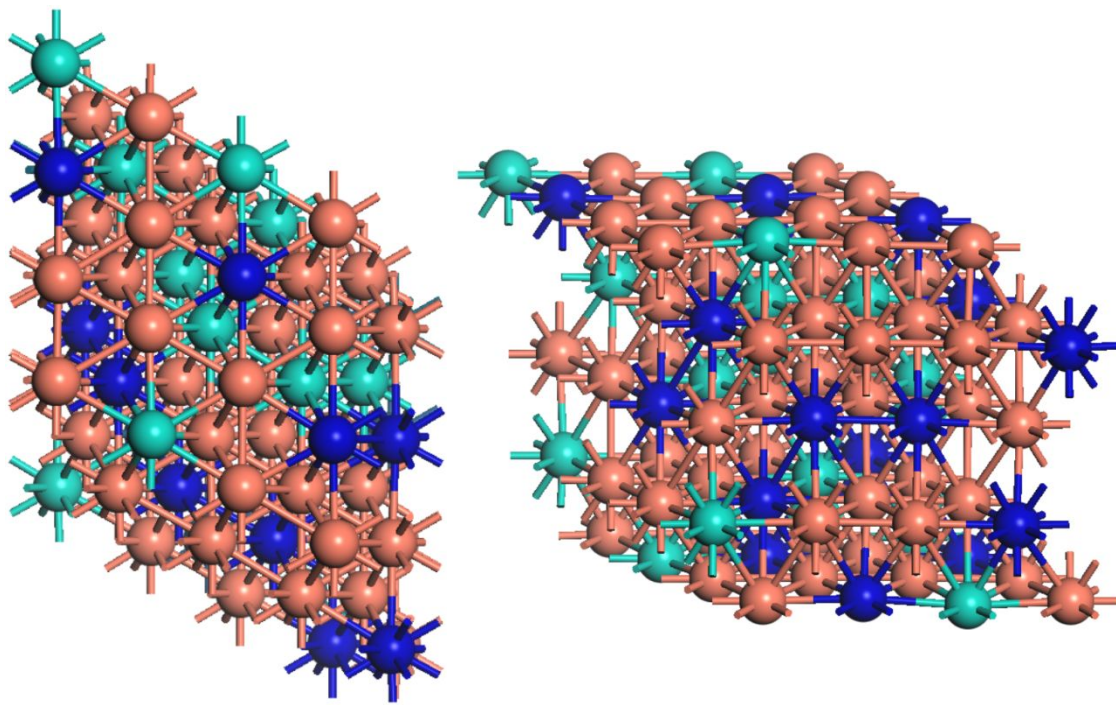


Fig. 2 The top view (left) and side view (right) of the model catalyst. Dark blue, blue, and brown balls represent Pt, Pd, and Cu atoms, respectively.

The exchange-correlation interactions were described using the Perdew-Burke-Ernzerhof (PBE) functional.³³ Projected augmented wave (PAW) potentials were used to depict the effective

core potentials of atoms.^{34, 35} A plane-wave basis set was used with a cutoff energy of 400 eV. A (2x2x1) Monkhost-Pack grid was used for the Brillouin zone. The convergence in optimization calculations was reached when the Hellmann-Feynman forces were less than 0.02 eV/Å. All the DFT calculations were carried out using VASP.^{36, 37} These DFT calculations are very similar to our previous work on the studies of trimetallic PtVFe catalysts,³⁸ bimetallic catalysts, CuPt/Pd^{39,}⁴⁰ and NiPd,⁴¹ and pure metal catalysts, Pd^{42, 43} and Cu.^{44, 45}

Based on the DFT energetics, we performed kinetics simulations for dissolution, deposition, and diffusions of Cu species. For all four processes, the rate constant (k) is calculated by the following general form with the parameters provided in the result and discussion:

$$k = Ae^{-\Delta G/RT}, \quad (1)$$

where A , ΔG , R , and T are the prefactor, activation free energy, gas constant, and temperature, respectively.

Results and discussion

Although trimetallic nanoparticles have been used as catalysts⁴⁶ and for sensing purposes,⁴⁷ studies on their stabilities are much lacking due to the complicated nature of the nanoparticles after a third element is introduced. In an attempt to understand the stability of trimetallic nanoparticles, in this work, we carried out DFT calculations on model catalysts with different surface compositions of PtPdCu(111) with a bulk composition of 18.75%(Pt), 18.75%(Pd), and 62.5%(Cu). Based on the DFT results, we then performed kinetics simulations for the dissolution, deposition, and diffusions from the first layer to the inner layer and from inner layer to the first layer of Cu species. The results are presented and discussed below.

Surface energy at various electrode potentials

Nanoparticle dissolution/deposition depends on many physicochemical factors, such as size, shape, composition.⁴⁸ As dissolution/deposition are closely related to the stability of nanoparticles, there are a lot of efforts being devoted to their studies, such as Cu₂O anodic dissolution,⁴⁹ dissolution and deposition of Cu⁵⁰ and other transition metals,⁵¹ and Ni-based nanofilms.⁵² Dissolution was also found to be dependent on pH,^{53, 54} bio condition for Au nanoparticles,⁵⁵ and morphology.⁵⁶ The driving force for dissolution/deposition of a nanoparticles at different electrode potentials can be divided into two parts. One is the direct driving force of the overpotential and the second is the chemical potential that is directly related to the surface energy of the nanoparticles. The surface energy changes with the electrode potential as different species can adsorb to the surface of nanoparticles and the ratio of facets can also be influenced. McCrum et al calculated the surface energies at different electrode potentials and their DFT results show the effect of electrode potential on the type and ratio of adsorbed species and the ratio of Pt(111), Pt(100), and Pt(110) surfaces,⁵⁷ which indicated that at electrode potentials of 0.2-0.8V, the bare surface energy for (111) surface can be used. We calculated the surface energy (γ) at the electrode potential (U) ranging from 0.8-1.2V based on the following equation:⁵⁷

$$\gamma(U) = \gamma_{bare} - \frac{2|e|U}{A}, \quad (2)$$

where γ_{bare} is the surface energy of the bare model catalyst surface with a surface area of A. We note that the electrode potential can also affect on surface energy through surface adsorption reactions that are neglected in this work, but would be interesting to future studies. The calculated surface energy of the model catalyst as a function of electrode potential is shown in Fig. 3.

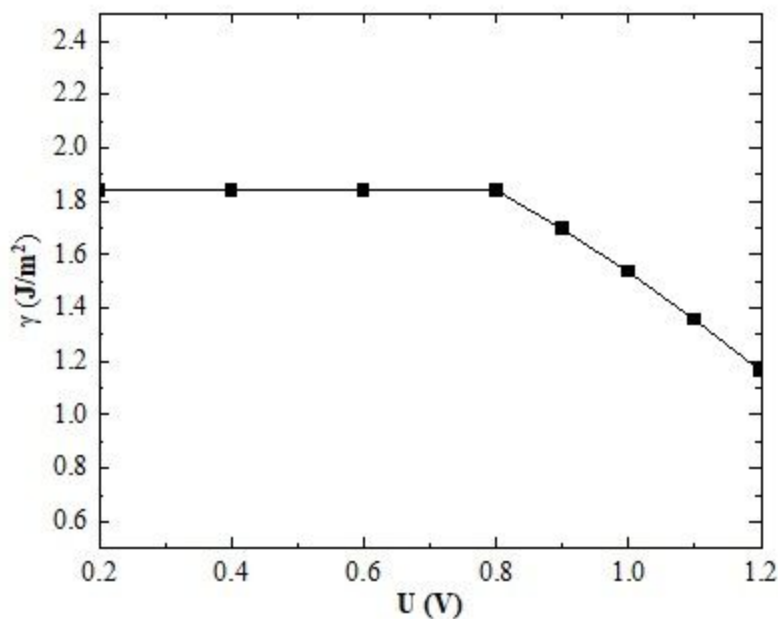


Fig. 3 Surface energy (γ) as a function of electrode potential (U) ranging from 0.2-1.2V. The surface energy is the same as the bare surface energy from 0.2-0.8V.

While the surface energies shown in Fig. 3 are for bare nanoparticles till 0.8 V and the effect of the adsorbed O species is added when the potential is above 0.8 V. In the kinetics simulations in this work, we used the surface energy at 0.9 V, which is the experimental condition.⁹ Also, the DFT calculations are for (111) surface only. Although the possibilities of other surfaces, i.e. (100) and (110), have increased at high potentials, (111) is the most dominant facet up to 1.2 V, which is the range of our concern. Furthermore, adsorbed O species of 0.25 monolayers is considered as the results show the most significance to the current study.²³ Therefore, we ignored the facet dependence of absorption, such as O₂ on Cu,^{58, 59} and others to simplify the investigation. We also point out that rate of dissolution/deposition depends on many factors, such as the size and shape of the catalysts, as well as solution.⁶⁰ Same size but different shape can create anisotropic character and therefore affect dissolution.⁶¹ Higher potentials also drastically increase the metal dissolution

rate.⁶² All the discussion mentioned above does not include the effect of reactions,⁶³ which could be important.

Composition of alloy nanoparticles does not only affect the surface energy, it also changes charge distributions of metals⁶⁴ and induce polarization.^{65, 66} Lattice constant is also affected by composition and can be used to identify the phase state of nanoparticles.⁶⁷ Different quantities, such as structure factor, coordination number,⁶⁸ cohesive energy, and excess energy²⁴ were developed to describe the homogeneity of bimetallic and trimetallic nanoparticles, it is experimentally difficult to synthesize specific type and too many calculations need to be carried out to have a holistic representation of the nanoparticles. Adsorbed ligand or solvent molecules on catalytic activities through influence of structure⁶⁹ and/or site density⁷⁰ and further increases the complexity. Nevertheless, three distinct cases can be studied and compared. Two extremes of segregation: one is Cu core and the second is the Cu skin. These core-shell structures are the best achievable cases by experiments to simultaneously control atomic arrangements in the bulk and on the surface.²⁸ Effect of core locations can affect the stability of nanoparticles.⁷¹ Inhomogeneity experiment on PtNi nanoparticles provided valuable information.²¹ A random selection of homogeneous alloying can also be studied, especially in the case of dilute alloys.⁷² Another important experiment is the examination of surface composition effect on the stability of nanoparticles¹⁹ and the results inspired this work to look into the effect of surface composition.

Dissolution and deposition of Cu species at various electrode potential

Dissolution of Cu atoms from the trimetallic nanoparticles is anodic reaction, i.e. $\text{Cu} \rightarrow \text{Cu}^{2+} + 2e^-$, and the rate constant was calculated using eq.(1), which is standard Butler-Volmer equation⁷³ with $A = 1.28 \times 10^{-4}$ cm/s. Anodic transfer factor of Cu is 0.29 for the surface.⁷⁴ We note that effective method of extracting kinetic parameters using differential Tafel plots was also

described.⁷⁵ For convenience, we used standard Cu potential in trimetallic alloy as that found in CuAu.⁷⁶ For deposition, we calculated the activation energy as a function of electrode potential and plotted in Fig. 4.

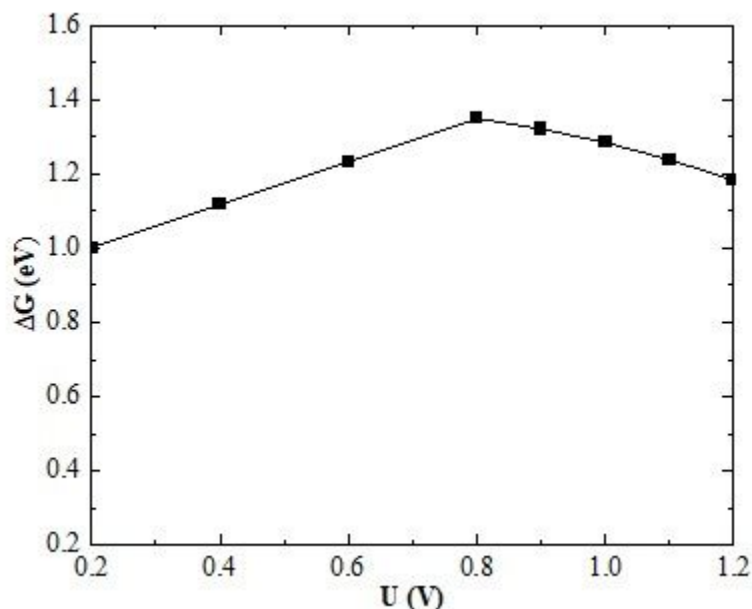


Fig. 4 Free energy difference (ΔG) as a function of electrode potential (U).

The free energy change, ΔG , is calculated²³ using

$$\Delta G = 2\beta(U - \phi^0) + \frac{2\gamma\Omega}{d}, \quad (3)$$

where β , ϕ^0 , Ω , and d denote the transfer factor, standard potential, atomic molar volume of Cu, and the radius of the nanoparticle, respectively. The adsorbed species also facilitate the formation of oxide and may also affect deposition.⁷⁷ The electrode potential affect the deposition process and therefore the morphology of nanoparticles. For instance, Ag nanoparticles will grow polyhedron at low potential but dendrite at high potential and nanosphere at extremely high potential.⁷⁸ Metal deposition also depends on size, curvature/film⁷⁹ and can be affected differently from the dissolution.

Diffusions of Cu atoms between the surface and the second layer of model catalyst

Diffusion of metal atoms in ternary alloys has been studied due to their importance in the properties of alloys. Anusavice and DeHoff used tracers, Cu⁶⁷, Ni⁶⁶, and Zn⁶⁵, to study the inter-diffusion of Cu rich alloys of CuNiZn.⁸⁰ Diffusion in solid⁸¹ and solid-state electrolytes of LiPS⁸² has received great attentions due to their role in many applications. Diffusion of a Cu atom in a nanoparticle such as the model catalyst can take place in two types: self-diffusion⁸³ and inter-diffusion. As self-diffusion does not change composition and is therefore not considered here. Inter-diffusion, in particular, diffusion between the surface layer the inner layer species, causes the change of surface composition and affect the stability of the nanoparticles. Inter-diffusion is often evaluated using diffusion couple technique.⁸⁴ The Boltzmann-Matano method is mostly used to determine the inter-diffusion coefficient as a function of concentration.⁸⁵

In this work, we studied the effect of diffusion of Cu atoms between the surface layer and the inner layers in the stability of Pt₂₀Pd₂₀Cu₆₀ nanoalloys. Particle size is not only important in catalytic performance,⁸⁶ it also affects the properties of nanoparticles⁸⁷ and the stability of nanoparticles. There are magic sizes on pure metal nanoparticles, such as Ir.⁸⁸ However, in this work, we considered the bulk (111) surface as a representative of the experimental nanoparticles.⁵⁷⁸⁹ Future work will include the size effect. Specifically, we performed DFT calculations of the model catalysts shown in Figure 2 with varying surface Cu compositions while we fixed the overall compositions. Specifically, we kept the total number of Cu, Pt, Pd atoms the same in the top two layers while varying the number of Cu atoms in the first layer. For instance, each layer of the model catalysts in Figure 2 consists of 3 Pt, 3 Pd, and 10 Cu, which corresponds to a surface Cu composition of 62.5%. In the surface Cu composition of 50%, there are 4 Pt, 3 Pd, and 8 Cu in the first layer and 2 Pt, 2 Pd, and 12 Cu in the second layer. As for the location of the different types

of atoms, we randomly chose one configuration in the calculation. The energy difference among different configurations are small based on our results on 4 randomly constructed catalyst models (One shown in Figure 2 and the other three in Figure S1 of the supporting information). The energy differences due to the surface composition are depicted in Fig. 5.

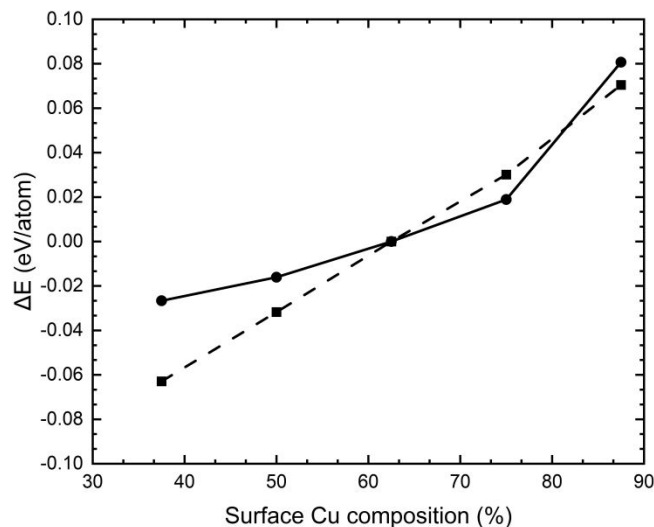


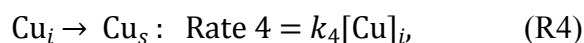
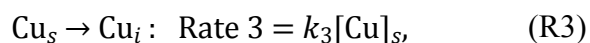
Fig. 5 Energy difference of the model catalyst as a function of surface Cu composition. The solid line represents data from relaxed structures and the dashed line from unrelaxed structures.

The DFT results shown in Fig. 5 show clearly that the nanoparticle becomes more stable with the decrease of Cu composition in the nanoparticles. This is consistent with the experimental observations that surface Cu composition is decreased after 20,000 cycles.⁹ The near linearity of the dependence also indicates that other processes or factors that favor Cu composition play a role, such as entropy effect. Although the difference indicates the energy difference between the Cu atoms occupy surface sites or inner layer sites, it adds to the activation energy to the Cu diffusion from the inner layer to the surface layer. In addition to surface composition, surface defects of nanoparticles can affect diffusion and deposition process as the adsorption of species in solvent will be changed, thus affecting the diffusion as well as deposition of Cu^{2+} .^{90, 91} Therefore, more

sampling of configurations is needed in the future studies to fully capture the effect of size, shape, and chemical ordering⁹² or even the support catalysts.⁹³ Inclusion of adsorbed species⁹⁴ and special adsorption configurations on a catalyst cluster⁹⁵ will also be interesting and important. In this work, we performed 16 DFT calculations to investigate the site dependence of O adsorption and the results are shown in Figures S2-S4 of supporting information. We also performed DFT calculations of 2 O, 3 O, and 4 O adsorption and the results are shown in Figure S5 of supporting information. These results illustrate that the adsorbed O species will stabilize the presence of Cu atoms.

Rates of dissolution, deposition, and diffusion of Cu species

To understand the roles of dissolution, deposition, and diffusion of Cu species, which is shown below, we performed kinetics calculations.



where subscript s and i denotes the composition of surface layer or the inner layer. The concentration of Cu^{2+} was set to be very low, 10^{-15} M. The four rate constants were calculated using eq.(1) and the values are provided in Table S1 of supporting information. Use the DFT energetics, we calculated the four rates as a function of Cu surface composition and the results are shown in Fig.6.

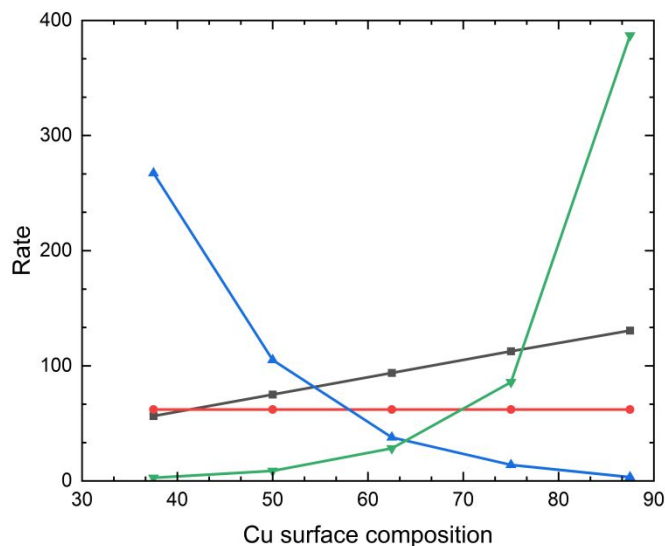


Fig. 6 Reaction rates (arbitrary unit) as a function of surface composition at $U=0.9V$ (vs RHE) and $T=298K$. Black, red, green, blue lines denote the dissolution (R1), deposition (R2), diffusion from surface to the inner layer (R3), and diffusion from the inner layer to the surface (R4), respectively.

Three observations can be made from the trends in Fig. 6. First, the Cu surface composition affects the rates differently. While dissolution and deposition are less dependent on the surface composition, diffusion are drastically dependent on the surface composition. Diffusion of Cu atoms from surface to the inner layer (green line) increases with increasing Cu surface composition, it is opposite for the diffusion from inner to surface layer. Second, at the initial Cu surface composition of 62.5%, dissolution/deposition processes are dominant. Interestingly, the diffusion from inner to the surface layer is slightly slower than the diffusion in opposition direction. Third, when the Cu surface composition is lower than 55%, diffusion becomes favorable. There is a dynamic Cu surface composition range that is determined by the interplay of the four processes.

Furthermore, the dynamic Cu composition range of 50-60% corresponds to an oscillation of lattice constants between 3.76 to 3.80 Å of the nanoparticles, which was observed experimentally.⁹ This indicates that the lattice constant oscillations shown experimentally could be due to the dynamic equilibrium achieved among dissolution of Cu species, diffusion of Cu atoms from inner

layer to surface layer, and deposition of Cu species. We also note that the limited random trimetallic models at one size (5.0 nm nanoparticle shown in Figure S6 of supporting information) are chosen in the current studies. Built upon the current results, future work is needed to consider the effects of shape, size,⁹⁶ chemical ordering,⁹⁷ adsorbed species at various compositions,⁹⁸ and utilization of neural network method⁹⁹⁻¹⁰¹ to incorporate the representations.

Conclusions

To understand the stability of experimentally observed highly active and durable ternary catalysts, PtPdCu nanoparticles, in this work, we carried out density functional theory (DFT) based computations to investigate the processes of dissolution, deposition, and diffusion between surface and inner layer of Pt₂₀Pd₂₀Cu₆₀ catalysts at electrode potentials up to 1.2 V. The kinetics results based on the DFT results show there is a dynamic Cu surface composition range that is determined by the interplay of the four processes, dissolution, deposition, diffusion from surface to inner layer, and diffusion from inner to surface layer of Cu species in the stability of the Cu-rich PtPdCu nanoalloys. Furthermore, this dynamic Cu surface composition range may be responsible to the experimentally observed oscillation of lattice constants of the Cu-rich PtPdCu nanoalloys. The methodology developed in this work can be used to study the stability of other binary or ternary nanoparticles and the results will provide benchmark for future in-depth studies of Cu-rich nanoalloys.

Author contributions

LW conceived the idea of the work, performed kinetics calculations, led data analysis, prepared figures, and wrote the manuscript with contributions from all authors. RMO performed extensive DFT calculations and prepared figures for the manuscript. PKJ developed nanoparticles of 5.0 nm, prepared figures for the manuscript, and performed DFT calculations. ZPW contributed to the

conception of the study, drew the draft of Fig. 1, and provided experimental insights. CJZ contributed to the conception of the study and provided experimental insights. All authors contributed to the discussion of the results and completion of the manuscript.

Conflicts of interest

The authors have no conflicts of interest to declare.

Acknowledgements

CJZ acknowledges the support from the US National Science Foundation (CHE 2102482).

References

1. L. Yaqoob, T. Noor and N. Iqbal, *RSC Adv.*, 2021, **11**, 16768-16804.
2. S. Ogo and Y. Sekine, *Fuel Process. Technol.*, 2020, **199**, 106238.
3. B. Miao, Z.-P. Wu, H. Xu, M. Zhang, Y. Chen and L. Wang, *Comput. Mater. Sci.*, 2019, **156**, 175-186.
4. R. Wu and L. Wang, *ChemPhysChem*, 2022, e202200132.
5. R. Wu and L. Wang, *Chem. Phys. Impact*, 2021, **3**, 100040.
6. R. Wu and L. Wang, *J. Phys. Chem. C*, 2020, **124**, 26953-26964.
7. R. Wu, K. R. Wiegand and L. Wang, *J. Chem. Phys.*, 2021, **154**, 054705.
8. R. Wu, K. R. Wiegand, L. Ge and L. Wang, *J. Phys. Chem. C* 2021, **125**, 14275-14286.
9. Z.-P. Wu, D. T. Caracciolo, Y. Maswadeh, J. Wen, Z. Kong, S. Shan, J. A. Vargas, S. Yan, E. Hopkins, K. Park, A. Sharma, Y. Ren, V. Petkov, L. Wang and C.-J. Zhong, *Nat. Commun.*, 2021, **12**, 859.
10. Y. Xue, L. Shi, X. Liu, J. Fang, X. Wang, B. P. Setzler, W. Zhu, Y. Yan and Z. Zhuang, *Nat. Commun.*, 2020, **11**, 5651.
11. R. Ma, G. Lin, Y. Zhou, Q. Liu, T. Zhang, G. Shan, M. Yang and J. Wang, *NPJ Comput. Mater.*, 2019, **5**, 78.
12. C. Hu and L. Dai, *Angew. Chem. Int. Ed.*, 2016, **55**, 11736-11758.
13. J. Zhang, Y. Yuan, L. Gao, G. Zeng, M. Li and H. Huang, *Adv. Mater.*, 2021, **33**, 2006494.
14. T. Wang, M. Park, Q. Yu, J. Zhang and Y. Yang, *Mater. Today Adv.*, 2020, **8**, 100092.
15. P. N. Plessow and F. Abild-Pedersen, *ACS Catal.*, 2016, **6**, 7098-7108.
16. Q. Wan, S. Hu, J. Dai, C. Chen and W.-X. Li, *J. Phys. Chem. C*, 2019, **123**, 11020-11031.
17. Y. Zhou, R. Pasquarelli, T. Holme, J. Berry, D. Ginley and R. O'Hayre, *J. Mater. Chem.*, 2009, **19**, 7830-7838.
18. L. Yang, S. Shan, R. Loukrakpam, V. Petkov, Y. Ren, B. N. Wanjala, M. H. Engelhard, J. Luo, J. Yin, Y. Chen and C.-J. Zhong, *J. Am. Chem. Soc.*, 2012, **134**, 15048-15060.
19. E. Pizzutilo, S. J. Freakley, S. Geiger, C. Baldizzone, A. Mingers, G. J. Hutchings, K. J. J. Mayrhofer and S. Cherevko, *Catal. Sci. Technol.*, 2017, **7**, 1848-1856.
20. A. Bergmann and B. R. Cuenya, *ACS Catal.*, 2019, **9**, 10020-10043.
21. Y.-C. Wang, T. J. A. Slater, G. M. Leteba, A. M. Roseman, C. P. Race, N. P. Young, A. I. Kirkland, C. I. Lang and S. J. Haigh, *Nano Lett.*, 2019, **19**, 732-738.
22. S. G. Rinaldo, W. Lee, J. Stumper and M. Eikerling, *Phys. Rev. E*, 2012, **86**, 041601.
23. J. Zhu, S. Hu, Z. Zeng and W.-X. Li, *J. Chem. Phys.*, 2019, **151**, 234711.
24. Z. Yan, M. G. Taylor, A. Mascareno and G. Mpourmpakis, *Nano Lett.*, 2018, **18**, 2696-2704.

25. L. Cao, Z. Zhao, Z. Liu, W. Gao, S. Dai, J. Gha, W. Xue, H. Sun, X. Duan, X. Pan, T. Mueller and Y. Huang, *Matter*, 2019, **1**, 1567-1580.
26. X.-L. Cai, C.-H. Liu, J. Liu, Y. Lu, Y.-N. Zhong, K.-Q. Nie, J.-L. Xu, X. Gao, X.-H. Sun and S.-D. Wang, *Nano-Micro Lett.*, 2017, **9**, 48.
27. A. Marcu, G. Toth, R. Srivastava and P. Strasser, *J. Power Sources*, 2012, **208**, 288-295.
28. M. Xie, Z. Lyu, R. Chen, M. Shen, Z. Cao and Y. Xia, *J. Am. Chem. Soc.*, 2021, **143**, 8509-8518.
29. A. Lu, Z.-P. Wu, B. Chen, D.-L. Peng, S. Yan, S. Shan, Z. Skeete, F. Chang, Y. Chen, H. Zheng, D. Zeng, L. Yang, A. Sharma, J. Luo, L. Wang, V. Petkov and C.-J. Zhong, *J. Mater. Chem. A*, 2018, **6**, 5143-5155.
30. H.-H. Li, C.-H. Cui, S. Zhao, H.-B. Yao, M.-R. Gao, F.-J. Fan and S.-H. Yu, *Adv. Energy Mater.*, 2012, **2**, 1182-1187.
31. J. Zhang, K. Sasaki, E. Sutter and R. R. Adzic, *Science*, 2007, **315**, 220-222.
32. X. Huang, Z. Zhao, L. Cao, Y. Chen, E. Zhu, Z. Lin, M. Li, A. Yan, A. Zettl, Y. M. Wang, X. Duan, T. Mueller and Y. Huang, *Science*, 2015, **348**, 1230-1234.
33. J. P. Perdew, K. Burk and M. Ernzerhof, *Phys. Rev. Lett.*, 1996, **77**, 3865-3868.
34. P. E. Blöchl, *Phys. Rev. B*, 1994, **50**, 17953-17979.
35. G. Kresse and J. Joubert, *Phys. Rev. B*, 1999, **59**, 1758-1775.
36. G. Kresse and J. Hafner, *Phys. Rev. B* 1993, **47**, 558-561.
37. G. Kresse and J. Furthmüller, *Phys. Rev. B*, 1996, **54**, 11169-11186.
38. L. Wang, J. I. Williams, T. Lin and C. J. Zhong, *Catal. Today*, 2011, **165**, 150-159.
39. R. Wu and L. Wang, *Comput. Mater. Sci.*, 2021, **196**, 110514.
40. R. Wu and L. Wang, *Chem. Phys. Lett.*, 2017, **678**, 196-202.
41. B. Miao, Z. Wu, M. Zhang, Y. Chen and L. Wang, *J. Phys. Chem. C*, 2018, **122**, 22448-22459.
42. Z.-P. Wu, S. Shan, Z.-H. Xie, N. Kang, K. Park, E. Hopkins, S. Yan, A. Sharma, J. Luo, J. Wang, V. Petkov, L. Wang and C.-J. Zhong, *ACS Catal.*, 2018, **8**, 11302-11313.
43. Z.-P. Wu, B. Miao, E. Hopkins, K. Park, Y. Chen, H. Jiang, M. Zhang, C.-J. Zhong and L. Wang, *J. Phys. Chem. C*, 2019, **123**, 20853-20868.
44. K. Sun, M. Zhang and L. Wang, *Chem. Phys. Lett.*, 2013, **585**, 89-94.
45. Z. Wu, M. Zhang, H. Jiang, C.-J. Zhong, Y. Chen and L. Wang, *Phys. Chem. Chem. Phys.*, 2017, **19**, 15444-15453.
46. J. W. M. Crawley, I. E. Gow, N. Lawes, I. Kowalec, L. Kaban, C. R. A. Catlow, A. J. Logsdail, S. H. Taylor, N. F. Dummer and G. J. Hutchings, *Chem. Rev.*, 2022, **122**, 6795-6849.
47. F. Nie, L. Ga, J. Ai and Y. Wang, *Front. Chem.*, 2020, **8**, 244.
48. S. K. Misra, A. Dybowska, D. Berhanu, S. N. Luoma and E. Valsami-Jones, *Sci. Total Environ.*, 2012, **438**, 225-232.
49. P. Zhou, M. J. Hutchison, J. R. Scully and K. Ogle, *Electrochim. Acta*, 2016, **191**, 548-557.
50. S. Pradhan, J. Hedberg, J. Rosenqvist, C. M. Jonsson, S. Wold, E. Blomberg and I. O. Wallinder, *PLOS one*, 2018, **13**, e0192553.
51. J. A. Gilbert, I. A. Shkrob and D. P. Abraham, *J. Electrochem. Soc.*, 2017, **164**, A389-A399.
52. L.-F. Huang, H. M. Ha, K. L. Cwalina, J. R. Scully and J. M. Rondinelli, *J. Phys. Chem. C*, 2019, **123**, 28925-28940.
53. L. Tang, X. Li, R. C. Cammarata, C. Friesen and K. Sieradzki, *J. Am. Chem. Soc.*, 2010, **132**, 11722-11726.
54. K. Wang, J. Han, A. Y. Gerard, J. R. Scully and B.-C. Zhou, *NPJ Mater. Degrad.*, 2020, **4**, 35.
55. U. Carlander, K. Midander, Y. S. Hedberg, G. Johanson, M. Bottai and H. L. Karlsson, *ACS Appl. Bio. Mater.*, 2019, **2**, 1006-1016.
56. Q. Wang, J. Liu, W. Zhang, T. Li, Y. Wang, H. Li and A. Cabot, *Inorg. Chem.*, 2022, **61**, 6337-6346.
57. I. T. McCrum, M. A. Hickner and M. J. Janik, *Langmuir*, 2017, **33**, 7043-7052.

58. R. Wu, K. Sun, Y. Chen, M. Zhang and L. Wang, *Surf. Sci.*, 2021, **703**, 121742.
59. M. M. Montemore, M. A. v. Spronsen, R. J. Madix and C. M. Friend, *Chem. Rev.*, 2018, **118**, 2816-2862.
60. W. Liu, J. Li, W. Li, H. Xu, C. Zhang and X. Qiu, *Nat. Commun.*, 2020, **11**, 3629.
61. K. Yuan, V. Starchenko, S. S. Lee, V. D. Andrade, D. Gursoy, N. C. Sturchio and P. Fenter, *ACS Earth Space Chem.*, 2019, **3**, 833-843.
62. J. Wandt, A. Freiberg, R. Thomas, Y. Gorlin, A. Siebel, R. Jung, H. A. Gasteiger and M. Tromp, *J. Mater. Chem. A*, 2016, **4**, 18300-18305.
63. L. Wang, C. Kalyanaraman and A. B. McCoy, *J. Chem. Phys.*, 1999, **110**, 11221-11232.
64. A. Cheng, R. Wang, Z. Liu, R. Liu, W. Huang and Z. Wang, *J. Phys. Chem. Lett.*, 2021, **12**, 8713-8719.
65. H. Zhang, M. Okumura and N. Toshima, *J. Phys. Chem. C*, 2011, **115**, 14883-14891.
66. W. Zhang, H. Zhao and L. Wang, *J. Phys. Chem. B*, 2004, **108**, 2140-2147.
67. S. Zhao, B. Zhao, X. Tian, Y. Ren, K. Yao, J. Wang, J. Liu and Y. Ren, *J. Phys. Chem. A*, 2017, **121**, 5226-5236.
68. W. Zhang, Q. Ge and L. Wang, *J. Chem. Phys.*, 2003, **118**, 5793-5801.
69. K. Spivey, J. I. Williams and L. Wang, *Chem. Phys. Lett.*, 2006, **432**, 163-166.
70. N. Smina, A. Rosen, L. Sztaberek, W. Beatrez, K. Kingsbury, R. Troia, Y. Wang, J. Zhao, J. Schrier and C. Koenigsmann, *ACS Appl. Mater. Interfaces*, 2021, **13**, 59892-59903.
71. M. Schnedlitz, R. Fernandez-Perea, D. Knez, M. Lasserus, A. Schiffmann, F. Hofer, A. W. Hauser, M. P. d. Lara-Castells and W. E. Ernst, *J. Phys. Chem. C*, 2019, **123**, 20037-20043.
72. K. G. Papanikolaou, M. T. Darby and M. Stamatakis, *ACS Catal.*, 2020, **10**, 1224-1236.
73. R. Guidelli, R. G. Compton, J. M. Feliu, E. Gileadi, J. Lipkowski, W. Schmickler and S. Trasatti, *Pure Appl. Chem.*, 2014, **86**, 245-258.
74. Q. Zhang, Z. Zhu, P. Liu, J. Zhang and F. Cao, *J. Electrochem. Soc.*, 2019, **166**, C401-C409.
75. P. Khadke, T. Tichter, T. Boettcher, F. Muench, W. Ensinger and C. Roth, *Sci. Rep.*, 2021, **11**, 8974.
76. D. K. Pattadar and F. P. Zamborini, *J. Phys. Chem. C*, 2019, **123**, 9496-9505.
77. H. Xu, B. Miao, M. Zhang, Y. Chen and L. Wang, *Phys. Chem. Chem. Phys.*, 2017, **19**, 26210-26220.
78. K. Wang, H. Huang and Y. Han, *Ind. Eng. Chem. Res.*, 2021, **60**, 14447-14454.
79. W. Schmickler, *Interfacial Electrochemistry*, Oxford University Press, 1996.
80. K. J. Anusavice and R. T. DeHoff, *Metall. Trans.*, 1972, **3**, 1279-1298.
81. T.-T. Fang, M.-I. Chen and W.-D. Hsu, *AIP Adv.*, 2020, **10**, 065132.
82. N. J. J. d. Klerk, E. v. d. Maas and M. Wagemaker, *ACS Appl. Energy Mater.*, 2018, **1**, 3230-3242.
83. G. D. Billing and L. Wang, *J. Phys. Chem.*, 1992, **96**, 2572-2575.
84. A. A. Kodentsov, G. F. Bastin and F. J. J. v. Loo, *J. Alloys Comp.*, 2001, **320**, 207-217.
85. T. Okino, *J. Mod. Phys.*, 2015, **6**, 2109-2144.
86. Q. Guan, C. Zhu, Y. Lin, E. I. Vovk, X. Zhou, Y. Yang, H. Yu, L. Cao, H. Wang, X. Zhang, X. Liu, M. Zhang, S. Wei, W.-X. Li and J. Lu, *Nat. Catal.*, 2021, **4**, 840-849.
87. D. Li, C. Wang, D. S. Strmcnik, D. V. Tripkovic, X. Sun, Y. Kang, M. Chi, J. D. Snyder, D. v. d. Vliet, Y. Tsai, V. R. Stamenkovic, S. Sun and N. M. Markovic, *Energy Environ. Sci.*, 2014, **7**, 4061-4069.
88. J. Lu, C. Aydin, N. D. Browning, L. Wang and B. C. Gates, *Catal. Lett.*, 2012, **142**, 1445-1451.
89. H. Lin, J.-X. Liu, H. Fan and W.-X. Li, *J. Phys. Chem. C*, 2020, **124**, 11005-11014.
90. V. Marinova, C. L. Freeman and J. H. Harding, *Faraday Discuss.*, 2022, DOI: 10.1039/d1fd00082a.
91. D. C. Clary and L. Wang, *J. Chem. Soc., Faraday Trans.*, 1997, **93**, 2763-2767.
92. J. Dean, M. J. Cowan, J. Estes, M. Ramadan and G. Mpourmpakis, *ACS Nano*, 2020, **14**, 8171-8180.
93. Y. Wang, Y.-Q. Su, E. J. M. Hensen and D. G. Vlachos, *ACS Nano*, 2020, **14**, 13995-14007.
94. T. S. Choksi, L. T. Roling, V. Streibel and F. Abild-Pedersen, *J. Phys. Chem. Lett.*, 2019, **10**, 1852-1859.
95. L. Wang, *Chem. Phys. Lett.*, 2007, **443**, 304-308.

96. L. Xiao and L. Wang, *J. Phys. Chem. A*, 2004, **108**, 8605-8614.
97. J. M. Rahm and P. Erhart, *J. Phys. Chem. C*, 2018, **122**, 28439-28445.
98. M. M. Sadek and L. Wang, *J. Phys. Chem. A*, 2006, **110**, 14036-14042.
99. Z. Xu, X. Shi, J. Li, S. Lu and L. Wang, *IEEE proceedings of 2009 Fifth International Conference on Natural Computation*, 2009, **1**, 86-90.
100. Z. Xu, S. Lu, J. Li and L. Wang, *IEEE proceedings of 2010 Sixth International Conference on Natural Computation*, 2010, **3**, 1586-1589.
101. J. A. Keith, V. Vassilev-Galindo, B. Cheng, S. Chmiela, M. Gastegger, K.-R. Müller and A. Tkatchenko, *Chem. Rev.*, 2021, **121**, 9816-9872.